Advanced image processing for defect visualization in infrared thermography

Yuri A. Plotnikov and William P. Winfree

NASA Langley Research Center, M.S. 231, Hampton, VA 23681-0001

ABSTRACT

Results of a defect visualization process based on pulse infrared thermography are presented. Algorithms have been developed to reduce the amount of operator participation required in the process of interpreting thermographic images. The algorithms determine the defect's depth and size from the temporal and spatial thermal distributions that exist on the surface of the investigated object following thermal excitation. A comparison of the results from thermal contrast, time derivative, and phase analysis methods for defect visualization are presented. These comparisons are based on three dimensional simulations of a test case representing a plate with multiple delaminations. Comparisons are also based on experimental data obtained from a specimen with flat bottom holes and a composite panel with delaminations.

Keywords: infrared thermography, image analysis, inverse problem, thermal tomography, nondestructive evaluations

1. INTRODUCTION

Recent achievements in thermal acquisition systems have led to improvements in the capabilities of thermographic methods for the nondestructive inspection of metallic and composite panels. In most cases pulsed transient thermography involves heating the surface of a target structure for a short period of time followed by the capture of the thermal decay using an infrared camera. Present-day systems enable the recording, storage, and processing of hundreds of digitized images at very fast rates. The thermal images are typically analyzed for the presence of hot spots which may indicate the existence of subsurface defects. Noise of multiple nature and optical distortions produce difficulties for the interpretation of the recorded data.

Post-processing is a powerful tool for the determination of the shapes and sizes of subsurface defects in inspected subjects. Regular video image analysis combined with special methods based on heat conduction theory can be applied to each scan stored in the computer memory. Several informative parameters of thermal response after heating realizing amplitude, temporal, and phase methods are currently used for enhancement of flaw images. The physical limitations of the informative parameters can be found by conducting analytical and numerical simulations of thermal flow propagation through a material.

In the present work different informative parameters for the task of defect shape extraction are compared. The comparison is based on results of a three-dimensional finite difference model of a solid body. The finite difference model simulates heat flow in a homogeneous plate with two square delaminations having different size and depth. Comparisons are also made on the basis of experimental data obtained from an aluminum specimen with flat bottom holes and a composite panel with delaminations.

2. FINITE DIFFERENCE MODEL

In many cases transient thermography could be simulated using one or two dimensions models. A useful and simple model is the disk-shape inclusion in cylindrical coordinates[1, 2, 3]. This model gives an accurate approximation of the thermographic inspection of a plate having a single defect. A limitation of this model is that it does not represent the presence of several defects with different geometry in observed area.

A three dimensions model allows to study edge effect and cross influence of the defects having different depth and size. An important advantage of three dimensions models is that it is easy to produce a sequence of two dimensions temperature

distribution from the model's surface. This sequence is similar to one received from an infrared camera, except it is free from noise, optical distortions, and heating inhomogeneouses. The usual thermal image processing technique can be applied to this "ideal" thermal response in order to study capabilities of thermal NDE.

A cross section of the model that is used for the mathematical simulations is illustrated in Fig. 1. The model is a 100 mm x 100 mm flat plate of thickness $D_z = 10mm$ with two delaminations. The delaminations are square form inclusions, 10 mm and 20 mm on a side, of thickness h = 0.2 mm located 2.4 mm and 7.4 mm below the surface respectively.

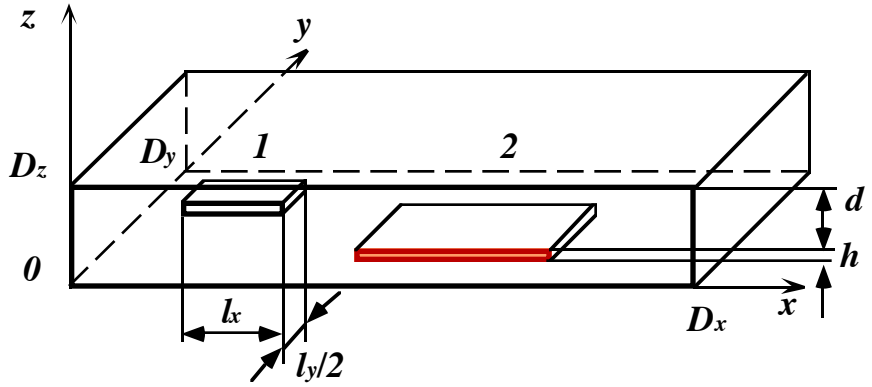

Fig. 1. Three-dimensional model of a plate containing two inclusions.

To simulate the thermographic inspection, the diffusion of heat after flash heating of the whole top surface has been modeled. The subsurface defects are represented as inclusions of a material with thermal properties different from the plate properties. The following assumptions have been made for the model. The plate is thermally insulated, convection and radiation losses from plate surface are neglected. The border $y = 0$ is modeled as insulated due to the symmetry of the system. The thermal properties of the plate and inclusions do not vary with temperature. With these assumptions temperature (above the ambient temperature) in the plate after pulse heating is governed by the unsteady heat diffusion equation

$$\frac{\partial T}{\partial t} = \alpha\left(\frac{\partial^2 T}{\partial x^2} + \frac{\partial^2 T}{\partial y^2} + \frac{\partial^2 T}{\partial z^2}\right), \tag{1}$$

where t is the time, α is the coefficient of thermal diffusivity and x, y, and z are Cartesian coordinates. At the beginning, the plate is in thermal equilibrium with the ambient temperature. The initial condition is expressed as

$$T(x, y, z, 0) = 0. \tag{2}$$

The boundary conditions at the insulated boundaries are

$$\left.\frac{\partial T}{\partial x}\right|_{x=0, x=D_x} = 0; \qquad \left.\frac{\partial T}{\partial y}\right|_{y=0, y=D_y} = 0; \qquad \left.\frac{\partial T}{\partial z}\right|_{z=0} = 0; \qquad \left.\frac{\partial T}{\partial z}\right|_{z=D_z} = \frac{Q}{K}, \tag{3}$$

where K is the thermal conductivity of the plate, Q is the surface heat flux. For defect-plate boundaries conditions are:

$$K\frac{\partial T}{\partial \vec{n}} = K_d\frac{\partial T_d}{\partial \vec{n}}; \qquad T = T_d, \tag{4}$$

where $\vec{n}$ is the normal vector to a defect surface, subscript d corresponds to area of the defects.

The size of the finite difference grid is 100 x 50 x 50 knots with geometrical size of 100 mm x 50 mm x 10 mm. It gives the spatial resolution of 1 mm in horizontal and 0.2 mm in vertical directions. By maintaining sample symmetry, only one half of the sample needs to be represented by the simulation. The boundary value problem (1)-(4) is solved by the simple explicit method [4]. The solution allows to have temperature value in every pixel of the grid for a moment of time from initial to infinity with time step Δt defined to have a stable solution[4].

The parameters of interest include the thermal contrast C, the time of the peak slope t_{ps} of the thermal contrast curve, and the phase φ of the Discrete Fourier transform applied to the temperature decay. The thermal contrast, the widely used in transient thermography analysis parameter, uses the difference between the thermal response of a flawless or sound region of a specimen and the region being inspected. In current work the contrast is defined as

$$C(t) = \frac{T_{def}(t) - T_{soa}(t)}{T_{soa}(t)}, \tag{5}$$

where $T_{def}(t)$ is the thermal response of the surface above the defect and $T_{soa}(t)$ is the thermal response of the sound area. The far right pixel on the plate surface (Fig. 1) has been used as the referent point of the sound area.

The time of peak slope has been found theoretically and experimentally as a stable characteristic of the defect depth[5, 6]. In the finite difference model this parameter is calculated as a moment of time when maximum difference between two following values of the thermal contrast $C(x, y, D_z, t + \Delta t) - C(x, y, D_z, t)$ occurs. Defined this way t_{ps} is accurate because of high precision and smoothness of the calculated contrast curve.

The phase images have been reported as reducing the effects of uneven surface heating and being highly sensitive to defects processing tool for nondestructive inspection[7, 8]. The phase is calculated as

$$\varphi = \arctan \frac{\mathrm{Im}}{\mathrm{Re}}, \tag{6}$$

where Im and Re are the imaginary and real components of the Fourier transform respectively. An advantage of the phase analysis is that it does not require the choosing of a reference point, which allows to reduce the operator's participation in the process of interpretation of the thermographic images.

3. ANALYSIS OF THE SIMULATED RESULTS

The finite difference model described above has been used in developing the computer program for the thermal response simulations. The calculations have been done on an UNIX Alpha station for thermal properties representing a carbon-epoxy plate (isotropic variant has been considered). Material properties for the inclusions have been chosen to represent Teflon and the air. For these materials the thermal resistance R of the inclusions calculated as h / K_d is 0.8 and $2.9 \times 10^{-3} m^2 K / W$ (Table 1). In order to spread out studied range of thermal resistance, an artificial case for a low conductive defect with $R = 200 \times 10^{-3} m^2 K / W$ has been also considered.
An instant surface heating is modeled by setting $Q = 100 kW / m^2$ in (3) for the first time step Δt and $Q = 0$ for following steps. The validity of the simulations has been verified by a comparison of the received temperature distributions with an analytical solution of adiabatic heating of the plate[9]. Good agreements have been received for simplified geometry of the model when the defects have the same thermal properties as the plate and when the defects have been stretched out to the plate borders.

The temperature distributions from the plate surface $z = D_z$ have been extracted from the complete solution. A time

Table 1. Thermal properties of materials used for the simulations.

Material	Conductivity	Diffusivity	Defect's resistance
Dimensions	[W/ m K]	[10^{-6} m^2/ s]	[10^{-3} m^2 K/ W]
Carbon-epoxy plate	5.4	2.8	-
Teflon inclusion	0.25	0.11	0.8
Air defect	0.07	0.58	2.9
Low conductive defect	0.01	0.01	200

evolution curve of the temperature for each knot on the surface has been constructed. Instead of analyzing the thermal contrast calculated for a certain moment of time, the summed contrast during the observation time t_{obs} has been analyzed. In order to cover all plate's depth, the observation time has been chosen from the condition $Fo = 1$, where $Fo = \alpha t / D_z^2$ is the Fourier number (normalized time). For our parameters $t_{obs} = 36s$. This period of time also has been used for the phase calculation. In present work the Fourier transform only for fundamental frequency has been calculated. In Fig. 2a-c the

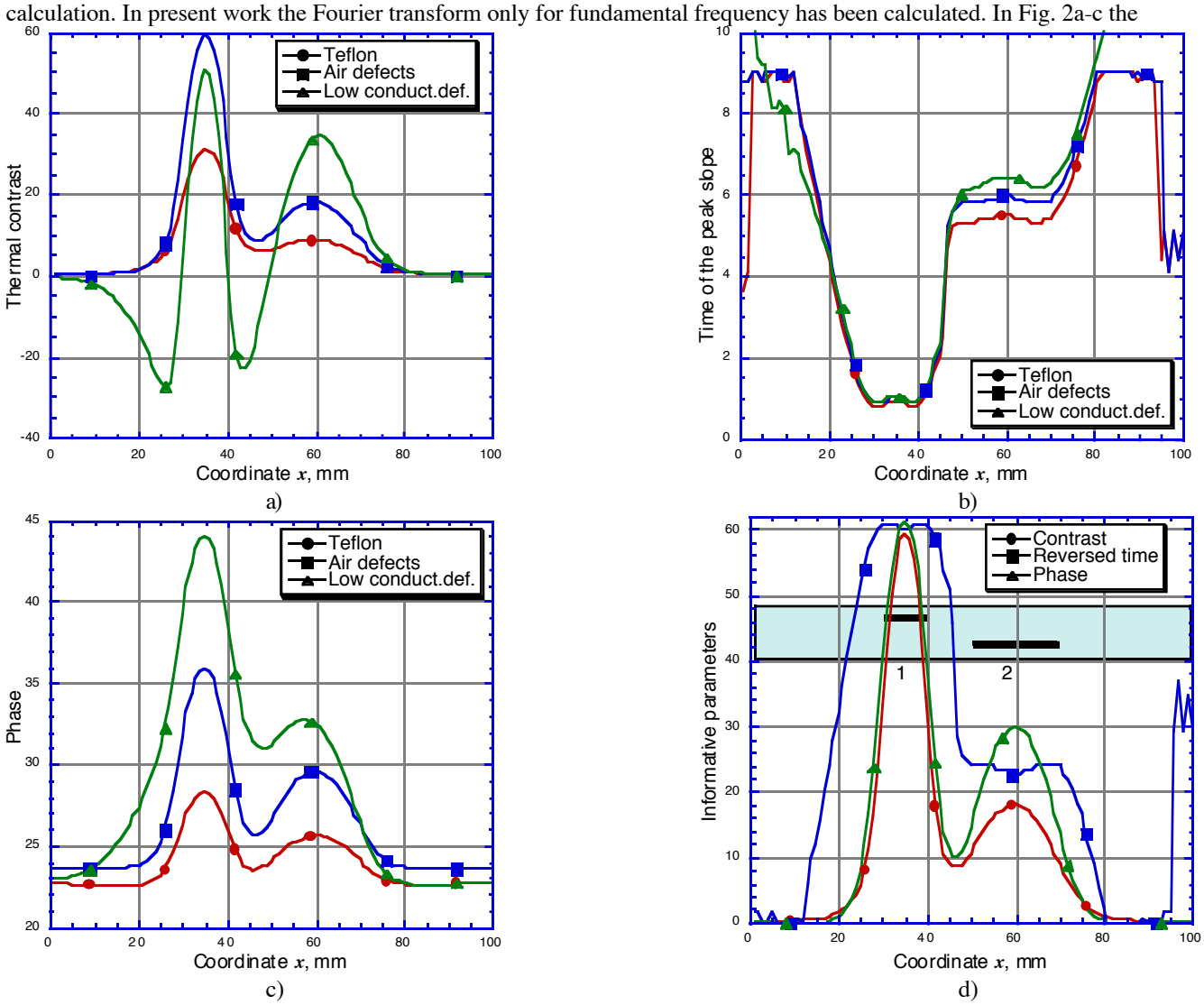

Fig. 2. Computed line profiles of the studied informative parameters above the centerline of the plate for the values of defect thermal resistance from Table 1. a) summed thermal contrast; b) peak slope time; c) phase of the discrete Fourier transform; d) the informative parameters for the air defects in the plate.

computed line profiles of the studied informative parameters are presented. The curves have been calculated above centerline of the defects where $y = 0$.

As can be seen from the Fig. 2a-c, all three informative parameters are sensitive to the variations of the defect depth and thermal resistance. The contrast and phase profiles have similar nature while the peak slope time one is different. It has the lowest sensitivity to the defect resistance variations. The difference is noticeable only for the deep defect. It feature makes this parameter very convenient for defect depth measuring. In addition, it is one of the fastest characteristics of the thermography (it requires for observation the period of time in four times less than for phase analysis).

For a comparison all three parameters for air defects scaled to fit each other are superimposed in Fig. 2d. For better comparability the reversed time of peak slope $8s - t_{ps}$ is presented. The time of peak slope profile has flat form directly above the defects. It makes possible the defect size extraction from this graph by setting a threshold level around flat parts of the profile. However, it is hard to design an automatic algorithm for this task if there are more than one defect in observation area. Two other graphs are more convenient for planar size extraction. The size of the defects in *xy*-plane can be calculated as a distance between steepest parts of the curves[1]. The planar distributions of the parameters in gray scale are shown in Fig. 3. All images clear indicate a presence of two defects. The edge effect is noticeable only for the temporal distribution.

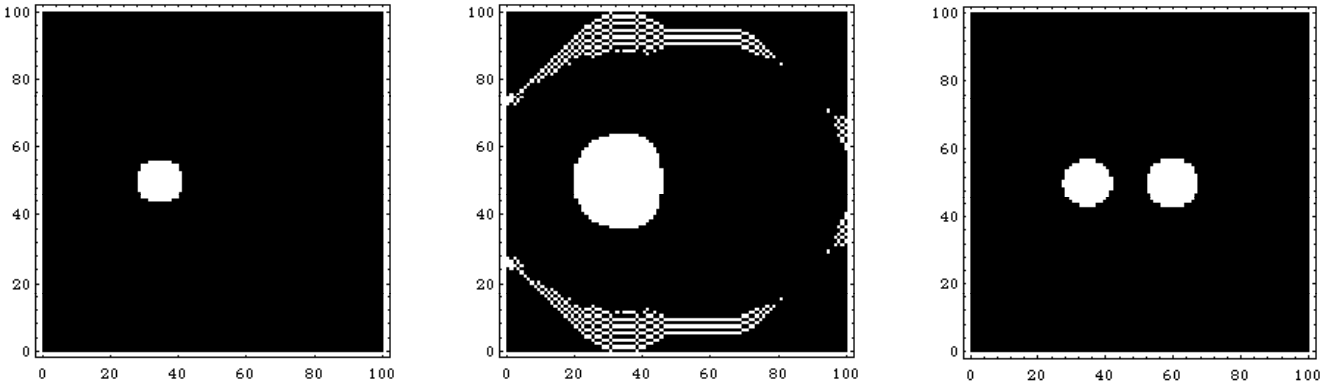

a) b) c)

Fig. 3. Surface distributions of the different parameters from Fig. 2d in gray scale. a) summed contrast; b) reversed time of the peak slope; c) phase image.

Analyzing the results, it can be concluded that the best solution is an application of two of these parameters simultaneously. The time of peak slope has better depth characterization while the contrast and phase images are more convenient for automatic planar size extraction. The application of temporal and contrast parameters has been previously proposed for thermal tomography algorithm[1].

4. EXPERIMENTS

The experimental part of this work has been done on aluminum and graphite-epoxy panels with artificial defects. The aluminum plate has size of 300 mm x 300 mm and thickness of 6 mm. Three square flat-bottom holes are milled into one side. They produce artificial defects having square cross section, 25 mm on a side, and located 0.7, 2.0, and 3.4 mm below the surface. Two flash lamps radiatively heat the surface of the specimen. A thermographic system based on an infrared imager with a single scanned HgCdTe detector collects surface radiation after heating in the 8-12 μm range. The digitized thermal response of the specimen is stored in a computer memory for further analysis. The series of 60 thermal images with size of 128 x 128 pixels received with sampling rate of 30 Hz has been used for calculation the parameters of interest. They have been calculated for a rectangular part of the images which contains 125 x 28 pixels and covers all three defects.

Experimentally obtained line profiles of the researched parameters across the defects scaled to fit each other are presented in Fig. 4a. All 60 values of the thermal response for each pixel in taken part of the images have been summed. A trend removal

procedure which uses pixels from the presumably free from defects perimeter of the partial image has been applied to this two-dimensional array. The resulting thermal contrast line profile produces a clear indication of the defects. The phase image has been computed for the fundamental frequency of 0.5 Hz using technique described in[7]. The reversed time of peak slope and phase profiles do not have a systematic trend. They show the defects, but have higher level of noise (Fig. 4a).

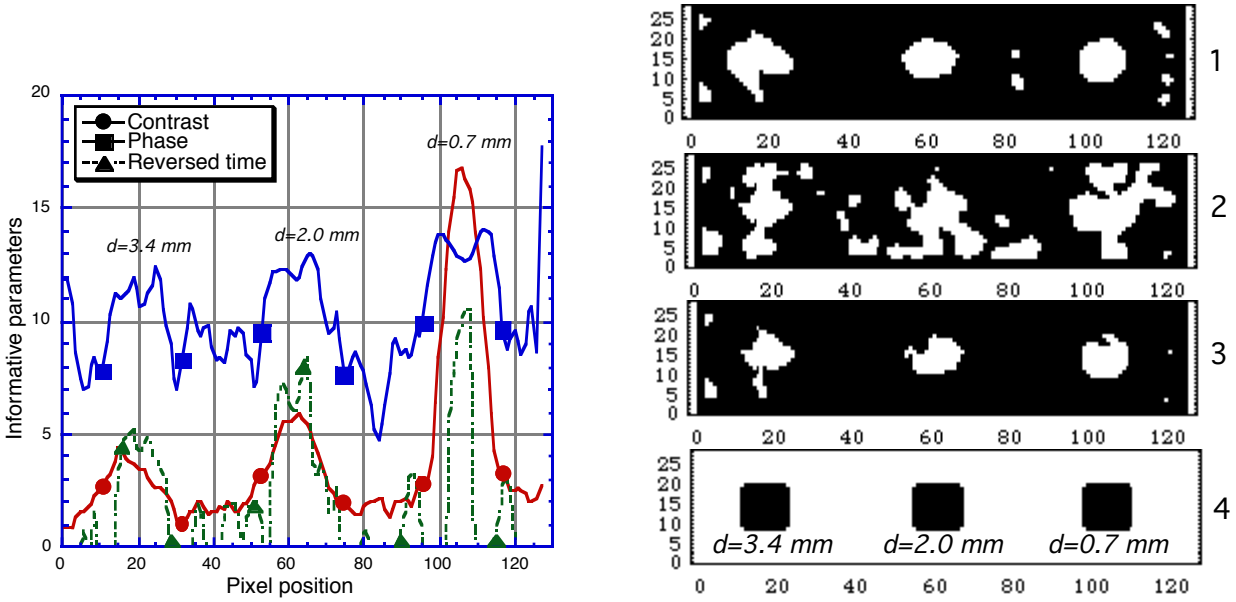

a) b)

Fig. 4. Experimental profiles of the researched parameters above the defect centerline in the aluminum plate (a) and binary images of the square voids in the plate (b). 1 - the binary map constructed from the contrast distribution; 2 - the binary map constructed from the phase distribution; 3 - the map derived from the upper pair by a multiplication; 4 - location of the flat-bottom defects in the observed area.

A defect edge extraction procedure based on an image gradient computation, which has been explained in details elsewhere[10], has been applied to the contrast and phase images. The resulting binary images of the defects are shown in Fig. 4b (images 1 and 2 respectively). Because of higher noise level in the original phase image, the derived binary image does not accurately represent the defects. The image 3 is a result of a multiplication of the contrast and phase binary images of the defects. The resulting image has less noise and a significant improvement in the correlation with the defect image 4 (Fig. 4b). A thermal tomography picture presented in Fig. 5 has been constructed using reversed time of the peak slope masked by

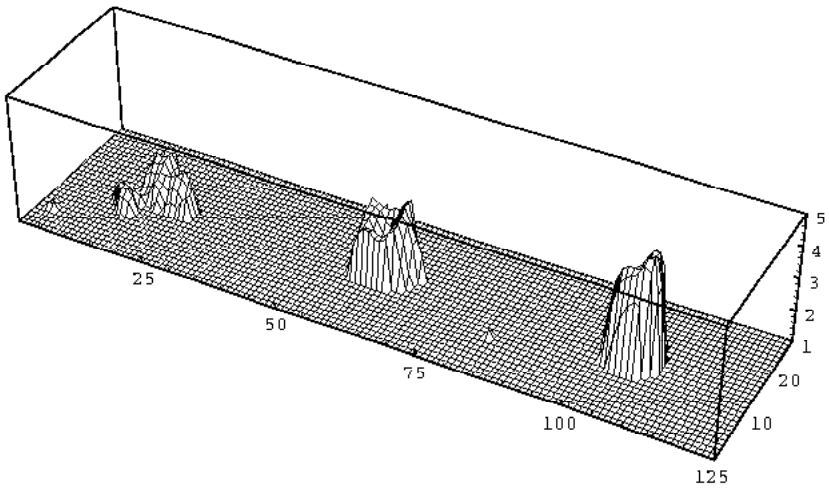

Fig. 5. 3D tomogram of the aluminum plate having three voids.

the binary contrast image. It gives a reasonable approximation of the defect depth. The tomogram covers area of the specimen approximately 240 mm x 54 mm.

The second sample is the graphite-epoxy composite panel having thickness of 3 mm with delaminations of different size and shape at the center of the composite[11]. The data acquisition procedure is similar to one for the aluminum plate. The series of 64 thermal images with size 256 x 256 pixels received with sampling rate of 10 Hz has been used for calculation the parameters of interest. A central part of the panel having 6 defects with size from 25 to 6 mm is analyzed in this work. The studied piece of the image contains 168 x 43 pixels.

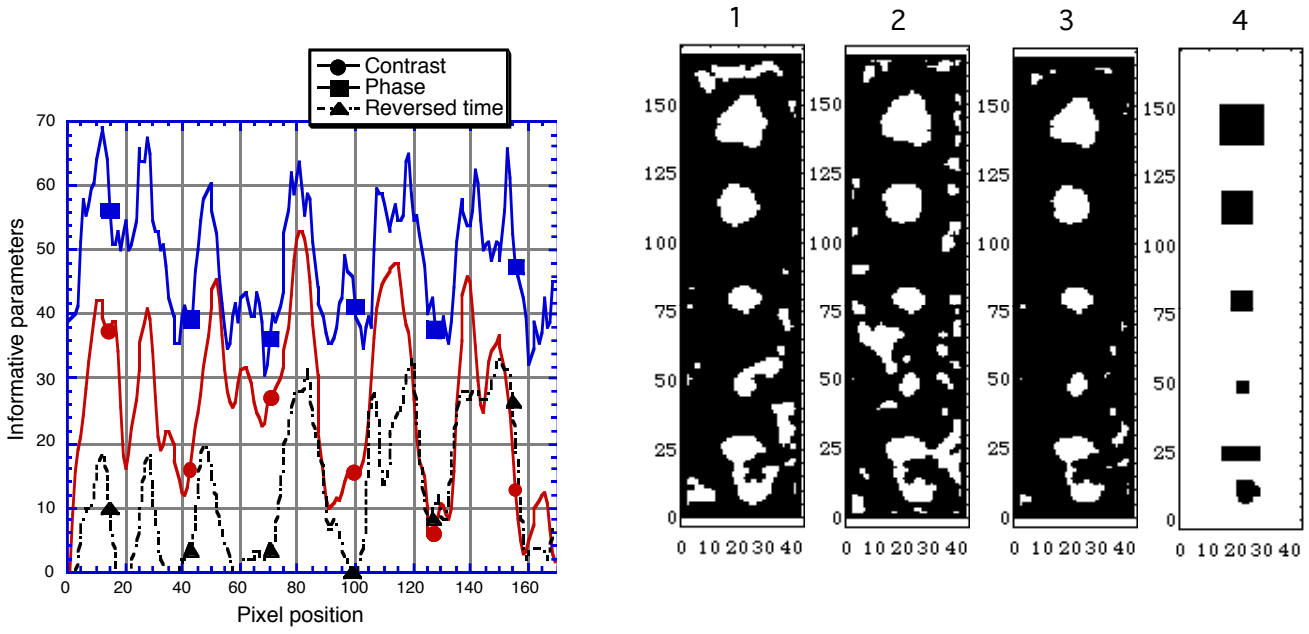

a) b)

Fig. 6. Experimental profiles of the researched parameters above defect centerline in the graphite-epoxy panel (a) and binary images of the delaminations in the plate (b). 1 - the binary map constructed from the contrast distribution; 2 - the binary map constructed from the phase distribution; 3 - the map derived from the images 1 and 2 by a multiplication; 4 - approximate geometry of the 6 delaminations in the observed area.

Experimentally obtained line profiles of the researched parameters across the defects scaled to fit each other are presented in Fig. 6a. The phase image has been computed for the fundamental frequency of 0.16 Hz. The thermal contrast summed during

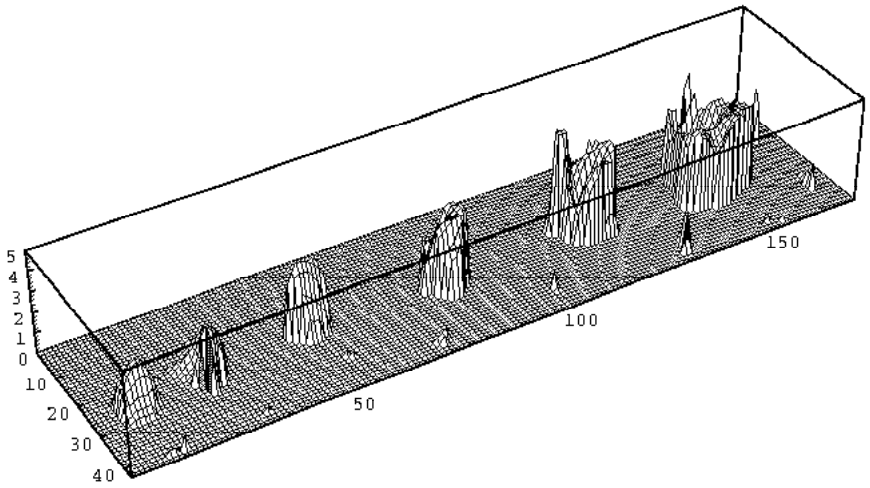

Fig. 7. 3D tomogram of the carbon-epoxy plate with six inclusions.

the observation time of 6.4 s produces a clear indication of the defects. The reversed time of peak slope and phase profiles also show the defects.

The binary images of the defects received from the contrast and phase images are shown in Fig. 6b (images 1 and 2). The image 3 is a result of a multiplication of the contrast and phase images of the defects. This derived image has lower noise level than each of the images 1 and 2 which indicates the complimentary feature of these two methods. The image 4 presenting the "true" location of the defects has been constructed using the input manufacturing draft and a thermal diffusivity measurement using a two side approach[11]. A thermal tomography picture presented in Fig. 7 has been constructed using the reversed time of the peak slope and the derived image 3 (Fig. 6b). The temporal distribution enhances the defects and reduces noise in surrounding area. The tomogram covers area of the specimen approximately 250 mm x 64 mm.

5. DISCUSSION AND FUTURE DIRECTIONS

Different informative parameters derived from image analysis have been used for the task of defect visualization. Results of mathematical simulations have shown that the most accurate reconstruction of the inner structure of a plate is obtained by combining thermal contrast or phase images and temporal characteristics of the thermal decay after pulse heating.

The thermal contrast is shown to be the most suitable parameter for the task of defect edge extraction. The time of the peak slope seems to be a good characteristic measure of defect depth. Pulse phase thermography has also been shown to be an effective method for edge extraction. Simultaneous usage of several informative parameters obtained from the same data set is a good way to produce a realistic size and depth reconstruction and reduce the noise. Further directions for research should include automation of each of the outlined processing procedures.

ACKNOWLEDGMENTS

This work was performed while author Plotnikov held a National Research Council - NASA Langley Research Center Research Associateship.

REFERENCES

1. X. Maldague, *Nondestructive Evaluation of Materials by Infrared Thermography*, London: Springer-Verlag, 1993.
2. V. Vavilov, X. Maldague, B. Dufort, F. Robitaille, and J. Picard, Thermal Nondestructive Testing of Carbon Epoxy Composites: Detailed Analysis and Data Processing, *NDT & E International*, Vol. 26, 2, 1993 pp. 85-95.
3. V.P. Vavilov, E. Grinzato, P.G. Bison, S. Marinetti, and C. Bressan, Thermal Characterization and Tomography of Carbon Fiber Reinforced Plastic Using Individual Identification Technique, *Materials Evaluation*, Vol. 54, May 1996, pp. 604-610.
4. W.J. Minkowicz, *Handbook of Numerical Heat Transfer*, New York: Wiley, 1988.
5. L.D. Favro, Xiaoyan Han, P.K. Kuo, and R.L. Thomas, Measuring Defect Depths by Thermal-wave Imaging, *in Thermosense XVIII: An International Conference on Thermal Sensing and Imaging Diagnostic Applications*, Proc. SPIE Vol. 2766, 1996, pp. 236-239
6. L.D. Favro, Xiaoyan Han, P.K. Kuo, and R.L. Thomas, Imaging the Early Time Behavior of Reflected Thermal-wave pulses, *in Thermosense XVII: An International Conference on Thermal Sensing and Imaging Diagnostic Applications*, Proc. SPIE Vol. 2473, 1995, pp. 162-166.
7. X. Maldague and S. Marinetti, Pulse Phase Infrared Thermography, *J. Appl. Phys.* 79 (5), 1996, pp. 2694-2698.
8. P.G. Bison, C. Bressan, G. Cavaccini, A. Caliberto, E.G. Grinzato, NDE of Composite Materials by Thermal Method and Shearography, *in Thermosense XIX: An International Conference on Thermal Sensing and Imaging Diagnostic Applications*, Proc. SPIE Vol. 3056, 1997, pp. 220-229.
9. H.S. Carslaw and J.C. Jaeger, *Conduction of Heat in Solids*, 2nd ed., Oxford: Oxford University Press, 1959.
10. Y.A. Plotnikov, W. P. Winfree, Thermographic Imaging of Defects in Anisotropic Composites, in: *D.O.Thompson and D.E. Chimenti (Eds.), Review of progress in QNDE*, Vol. 17, N.Y.: Plenum Press, (1998, in press).
11. W.P. Winfree, Enhanced Thermographic Detection of Delaminations with Computational Pulse Shaping, in: *D.O. Thompson and D.E. Chimenti (Eds.), Review of progress in QNDE*, Vol. 17, N.Y: Plenum Press, (1998, in press).